Hindawi
Journal of Nanomaterials
Volume 2020, Article ID 7180613, 15 pages
https://doi.org/10.1155/2020/7180613

Research Article

A Combination Therapy of pHRE-Egr1-HSV-TK/Anti-CD133McAb-^{131}I/MFH Mediated by FePt Nanoparticles for Liver Cancer Stem Cells

Mei Lin,[1] **Yanhong Xiao**,[2] **Xingmao Jiang**,[3] **Jun Zhang**,[4] **Ting Guo**,[5] **and Yujuan Shi**[2]

[1]*Clinical Laboratory, Taizhou People's Hospital Affiliated to Nantong University, Taizhou, Jiangsu 225300, China*
[2]*Imaging Department, Taizhou People's Hospital Affiliated to Nantong University, Taizhou, Jiangsu 225300, China*
[3]*Hubei Key Lab of Novel Reactor & Green Chemical Technology, Key Laboratory for Green Chemical Process of Ministry of Education, School of Chemical Engineering and Pharmacy, Wuhan Institute of Technology, Wuhan 430205, China*
[4]*Isotopic Laboratory, Taizhou People's Hospital Affiliated to Nantong University, Taizhou, Jiangsu 225300, China*
[5]*Institute of Clinical Medicine, Taizhou People's Hospital Affiliated to Nantong University, Taizhou, Jiangsu 225300, China*

Correspondence should be addressed to Mei Lin; l_mei@163.com

Received 3 February 2020; Revised 13 April 2020; Accepted 24 April 2020; Published 12 June 2020

Guest Editor: Anuj Kumar

It has been evidenced that liver cancer stem cells (LCSCs) are to blame hepatocellular carcinoma (HCC) occurrence, development, metastasis, and recurrence. Using iron-platinum nanoparticles (FePt-NPs) as a carrier and CD133 antigen as a target, a new strategy to targetly kill LCSCs by integrating HSV-TK suicide gene, ^{131}I nuclide irradiation, and magnetic fluid hyperthermia (MFH) together was designed and investigated in the present study. The results showed that FePt-NPs modified with PEI (PEI-FePt-NPs) could bind with DNA, and the best binding ratio was 1 : 40 (mass ratio). Moreover, DNA binding to PEI-FePt-NPs could refrain from Dnase1 enzyme digestion and could release under certain conditions. LCSCs ($CD133^+$ Huh-7 cells) were transfected with pHRE-Egr1-HSV-TK by PEI-FePt-NPs, and the transfection efficiency was 53.65 ± 3.40%. These data showed a good potential of PEI-FePt-NPs as a gene transfer carrier.^{131}I was labeled with anti-CD133McAb in order to facilitate therapy targeting. The combined intervention of pHRE-Egr1-HSV-TK/anti-CD133McAb-^{131}I/MFH mediated by PEI-FePt-NPs could greatly inhibit LCSCs' growth and induce cell apoptosis *in vitro*, significantly higher than any of the individual interventions ($p < 0.05$). This study offers a practicable idea for LCSC treatment, and PEI-FePt-NPs may act as novel nonviral gene vectors and a magnetic induction medium.

1. Introduction

As an extremely malignant tumor, hepatocellular cell carcinoma (HCC) severely endangers human health and life. There were about 800 thousand people that died of HCC all over the world in every past year [1, 2]. In the past decades, much progress has been made in hepatoma diagnosis and treatment, but the overall prognosis of HCC is still not satisfactory and the 5-year survival rate is only 10% or so. It is therefore pivotal to seek an effective strategy for HCC therapy.

In recent years, cancer stem cell (CSC) theory has drawn wide attention from scholars in the whole world [3]. Specifically, CSCs, accounting for merely 5% of tumor cells, are the root of tumor heterogeneity, with the ability for self-renewal, unlimited proliferation, and multidirectional differentiation potential. Normally, most of them exist in the G0 and hypoxic microenvironment, resistant to radiotherapy and chemotherapy in a way. Moreover, they are mostly to blame for the occurrence, progress, metastasis, and recurrence of tumor. CSCs have been discovered in blood malignant tumors and many solid tumors, such as breast cancer, colorectal cancer, HCC, lung cancer, pancreatic cancer, and multiple myeloma [4–10].

According to CSC theory, it is significant to eliminate liver cancer stem cells (LCSCs), which can be served as one

of the crucial indicators to monitor HCC progress and evaluate curative effect, for HCC treatment and prognosis improvement. Now, LCSCs are mainly isolated by flow cytometry and immune magnetic bead, the principles of which are both based on some specific markers to identify LCSCs. Many molecular markers of LCSCs have been discovered, including ALDH, CD133, CD13, CD90, CD44, CD24, OV6, and EpCAM. CD133, a five-transmembrane single-chain glycoprotein known as prominin-1, was first identified from human hematopoietic stem cells and mouse $CD34^+$ neural stem cells in 1997. It has been proved that $CD133^+$ HCC cells have the ability for proliferation, differentiation, and self-renewal. Suetsugu et al. [11] isolated $CD133^+$ cells from the Huh-7 cell line, which have a stronger ability to proliferate than $CD133^-$ Huh-7 cells *in vitro*. Hence, it has become a key research hotspot to integrate various means to specifically kill LCSCs in HCC therapy.

As a green therapy, tumor hyperthermia has shown ideal potential, and the techniques for thermotherapy have been continuously improved in recent years. Jordan et al. [12] developed magnetic fluid hyperthermia (MFH) for cancer treatment by integrating nanotechnology and magnetic induction hyperthermia together and achieved remarkable results. Specifically speaking, after delivery into the tumor area, magnetic fluid (contains magnetic nanoparticles) can warm up to the temperature capable of killing cancer cells by the rearrangement mechanism of the relaxation magnetic vector in an applied magnetic field (AMF). For the surrounding normal tissues, they are not adversely impacted without magnetic materials there, which makes the therapy highly targeted and specific. Furthermore, hyperthermia can not only directly kill tumor cells but also enhance the sensitivity of radiotherapy and chemotherapy.

Radiation-gene therapy is a strategy to combine a therapeutic gene with a radiation-inducible regulatory sequence to form recombinant plasmids. After transfection into tumor cells and administration of radiation, the therapeutic genes are induced to express themselves, resulting in a double kill of the tumor by radiation and the genes. In this regard, this method can relatively lower the equivalent irradiation dose and the damage to normal tissues, by which therapeutic genes can express locally by local irradiation as well. However, two key factors are involved in the desired therapeutic effect, with one being an applicable vector to transfer the therapeutic genes and the other gene expression regulation.

In view of the above background, exploiting CD133 antigen as a target, using PEI-FePt-NPs as a gene transferring carrier and magnetic thermotherapy medium, taking advantage of the solid tumor hypoxic microenvironment, we integrated anti-CD133McAb (anti-CD133 monoclonal antibody) labeled with ^{131}I, pHRE-Egr1-HSV-TK (suicidal genes driven by hypoxia/radiation double sensitive promoters), and MFH together, complementing their advantages, to kill LCSCs in the present study and obtained encouraging results.

2. Methods

2.1. Main Materials. The main materials are as follows: Huh-7 cell line (human HCC cells) (Shanghai Institute of Cell Research, Chinese Academy of Sciences), chloroplatinic acid (Chinese medicine), ferric nitrate (Chinese medicine), sodium chloride, (Chinese medicine), trimethylammonium bromide (CTAB) (Chinese medicine), polyethyleneimine (PEI) (Sigma, USA), dimethyl sulfoxide (Beijing Suo Laibao Technology Company), MTT (Sigma, USA), 0.25% trypsin-EDTA (Gibco, USA), DMEM (Gibco, USA), newborn bovine serum (Hangzhou Sijiqing Bioengineering Materials Research Institute), chloramine T (Sinopharm Chemical Reagent Co. Ltd.), $Na^{131}I$ (Gangwon Hospital), sodium sulfite (Sinopharm Chemical Reagent Co. Ltd.), BSA (Sinopharm Chemical Reagent Co. Ltd.), CD133 monoclonal antibody (ImmunoWay, USA), FcR Blocking Reagent (Miltenyi Biotec, Germany), epidermal growth factor (EGF) (PeproTech, USA), basic fibroblast growth factor (bFGF) (PeproTech Company, USA), insulin (PeproTech, USA), B27 (PeproTech, USA), DMEM/F12 medium (Gibco, USA), DNA marker (Shanghai Shenggong), PCR expansion additive kit (Shanghai Shenggong), Annexin V (Invitrogen), and propidium iodide (PI) (Invitrogen).

2.2. Sorting, Identification, and Culture of $CD133^+$ Huh-7 Cells. CD133 expression of Huh-7 cells was detected by flow cytometry. $CD133^+$ Huh-7 cells were sorted by flow cytometry and cultured in serum-free DMEM/F12 medium with 40 ng/ml EGF, 20 ng/ml bFGF, 1% B27, 0.4% bovine serum albumin, and 5 mg/ml insulin. The medium was replaced half every 3 days. The clone spheres were checked by a light microscope.

Soft agar cloning experiment process is as follows: (1) $CD133^+$ Huh-7 cells were trypsinized into individual cells at 1×10^6 cells/l with DMEM of 20% FBS. (2) Two low-concentration agarose solutions of 1.2% and 0.7% were prepared with dH_2O and placed at 40°C of water bath after autoclaving. (3) 1.2% agarose and 2× DMEM (containing 20% fetal bovine serum and 2 times double antibody) were mixed at 1 : 1 in a dish. After cooling coagulation, the mixture was placed in a CO_2 incubator to be used as bottom agar. (4) 0.7% agarose and 2 × DMEM were mixed at 1 : 1, and then, 0.2 ml cell suspension was added. After thoroughly mixing, the mixture was poured into the plate with a 1.2% agarose bottom layer; then, a double-layer agar medium was gradually formed. Placed in a biosafety cabinet after condensation, the cells were cultured in a 37°C, 5% CO_2 incubator for 12 days. (5) The cell clones in the plate were observed by an inverted microscope.

2.3. FePt-NP Synthesis, Modification, and Characterization. FePt-NPs were synthesized by reverse microemulsion method as follows. 0.087 g $Fe(NO_3)_3{\cdot}9H_20$, 0.1 g NaCl, and 5 ml $H_2PtCl_6{\cdot}6H_2O$ (0.02 g/ml) were dissolved in a conical flask, and 0.73 g CTAB and 90 ml benzene were added. Then, the mixture was mixed on a magnetic stirrer at 70°C for 6 h and then continued to be magnetically mixed at 90°C for 3 h. Subsequently, the water was removed, and the reminder mixture was dried and calcined in an air atmosphere for 5 h, then reduced in an H_2 atmosphere for 10 h. After washed with water to remove redundant NaCl and dried, FePt-NPs were obtained.

Some FePt-NPs were dissolved in deionized water to prepare 4% magnetic fluid, by ultrasonical dispersion. After

high-speed centrifugation, the supernatant was removed. The precipitate was resuspended in PBS and ultrasonically dispersed. Then, some PEI was slowly added to the mixture. The mass ratio of PEI to FePt-NPs is 1 : 5. After fully mixing and shaking for 24 h at room temperature, the nanoparticles were isolated by magnetic separation and washed repeatedly with distilled water and methanol, and then dried in vacuum to obtain FePt-NPs modified with PEI (PEI-FePt-NPs).

Some FePt-NPs were taken and dispersed in absolute ethanol for 15 min, respectively, then dropped to a copper mesh and observed under a transmission electron microscope (TEM, JEM-2100 (HR)). The morphology, size, and dispersion of FePt-NPs were checked and photographed, and then, a bar was marked in view of magnification in each picture. We counted 100 nanoparticles and calculated their size according to the bar, then figured out the mean and standard deviation (SD), applying mean ± SD.

X-ray diffraction (XRD) of FePt-NPs was detected in the condition of Cu targeting Kα ($\lambda = 0.154$ nm), 30 mA tube flow, and 40 kV tube pressure.

The magnetic fluids of FePt-NPs and PEI-FePt-NPs were prepared, respectively, and were placed at 4°C for one week to observe colloidal stability.

To detect magnetothermal effect, 0.25, 1.0, 1.5, and 2.0 g/l FePt-NP and PEI-FePt-NP magnetic fluids were prepared with 0.9% NaCl, respectively. Then, 5 ml of each magnetic fluid was put into a 25 cm^2 flat-bottomed test tube, respectively, and heated on the plate coil of high-frequency magnetic induction heating (SPG-10A-II) with 215 kHz frequency and 35 A output current at room temperature for 1 h. The test tube bottom was away about 0.5 cm from the heating coil center. The temperature was recorded every 5 min. Taking time as the abscissa and temperature as the ordinate, temperature rising curves of FePt-NP and PEI-FePt-NP magnetic fluids with different concentrations were drawn.

With 215 kHz and output currents 25 A, 30 A, 35 A, 40 A, 5 ml of 1.0 g/l FePt-NPs and PEI-FePt-NPs was heated for 1 h at room temperature as the above, respectively. Every five minutes, the temperature was recorded. Taking time as the abscissa and temperature as the ordinate, temperature rising curves of FePt-NP and PEI-FePt-NP magnetic fluids at different magnetic intensities were drawn.

2.4. Construction and Identification of Eukaryotic Expression Plasmids pHRE-Egr1-HSV-TK. Eukaryotic expression plasmids pCDNA3.1-pHRE-Egr1-HSV-TK (pHRE-Egr1-HSV-TK) were designed and constructed as References [13–17]. pHRE-Egr1-HSV-TK were digested by BglII+XhoI and then subjected to 1% agarose gel electrophoresis. The electrophoresis band was observed by a UV lamp. In addition, a 5HRE-Egr1 fragment in pCDNA3.1-5HRE-Egr1-HSV-TK was sequenced and then aligned with a 5HRE-Egr1 template sequence to further examine whether the plasmids were correctly constructed.

2.5. The Investigation of the Potential of PEI-FePt-NPs Used for Gene Transfer Carrier. Using pHRE-Egrl-EGFP constructed according to References [13–17] as a model, the potential of PEI-FePt-NPs used for gene transfer carrier was investigated.

2.5.1. Experiment of DNA Binding to PEI-FePt-NPs. PEI-FePt-NPs and pHRE-Egrl-EGFP were mixed at a mass ratio of 0 : 1, 5 : 1, 10 : 1, 20 : 1, 40 : 1, and 80 : 1, respectively, and the final concentration of plasmids was 20 ng/μl, then supplemented to 20 μl of total volume with ultrapure water, and placed at room temperature for 30 min to form a complex. 5 μl of each complex was taken for agarose gel electrophoresis (100 ng/lane) to detect the binding of DNA to a magnetic nanoparticle. And then, the most suitable ratio of pHRE-Egr1-EGFP binding to FePt-NPs was screened out.

2.5.2. The Experiment of Protection DNA from DNase1 Digestion by PEI-FePt-NPs. The complex of pHRE-Egrl-EGFP and PEI-FePt-NPs (1 : 40 of mass ratio) was mixed in Tango Buffer (Thermo) and DNase1 enzyme. After digestion for 1 min, 10 min, 30 min, 45 min, and 1 h at 37°C of water bath, the reaction was terminated by an equal volume of 0.5 mol/l EDTA solution, and DNase1 was further inactivated by a 55°C water bath. Then, pHRE-Egrl-EGFP binding to PEI-FePt-NPs was eluted with SDS, extracted with phenol and chloroform, precipitated with absolute ethanol, washed with 75% ethanol, and dissolved in equal double distilled water. Finally, agarose gel electrophoresis was performed to observe the ability of the complex to resist DNA enzymatic hydrolysis, and naked pHRE-Egrl-EGFP was used as a control.

2.5.3. The Examination of DNA Release from the Complex PEI-FePt-NPs/DNA. The total volume of the complex (mass ratio of pHRE-Egrl-EGFP and PEI-FePt-NPs was 1 : 40) was supplemented to 500 μl with TE solution for 10 μg plasmids, then shaken with 200 rpm at 37°C. An equal sample was taken out at hour 1, hour 4, hour 8, hour 12, day 1, day 2, day 3, and day 4, respectively, and subjected to agarose gel electrophoresis to observe DNA release from the complex.

2.5.4. The Detection of PEI-FePt-NP Gene Transfection Efficiency. PHRE-Egrl-EGFP was transfered into $CD133^+$ Huh-7 cells by PEI-FePt-NPs, and the transfection efficiency was tested and compared with the lipofection method. In detail, PEI-FePt-NPs and pHRE-Egrl-EGFP were diluted with serum-free medium at a mass ratio of 40 : 1 (according to the results of Section 2.5.1), respectively. 5 min later, the two were mixed and incubated for 30 min to obtain the pHRE-Egrl-EGFP/PEI-FePt-NP complex. The logarithmic growth phase $CD133^+$ Huh-7 cells were seeded in 6-well plates (5×10^5 cells/well) and cultured in 5% CO_2 at 37°C for about 18 h. Then, the original culture solution was discarded, and the cells were washed three times with sterile PBS and serum-free medium 2 times, respectively; then, serum-free medium containing pHRE-Egrl-EGFP/PEI-FePt-NPs complex (3 μg pHRE-Egrl-EGFP per well) were added to the corresponding wells. 5 h incubation later, the whole medium was replaced with serum-free. After the cells were routinely cultivated for 2 days, the transfection efficiency was detected by flow cytometry. As the control, pHRE-Egrl-EGFP was transfected into $CD133^+$ Huh-7 cells by liposome.

2.6. The Intervention of LCSCs by pHRE-Egr1-HSV-TK/Anti-CD133McAb-^{131}I/MFH In Vitro. ^{131}I-anti-CD133McAb were prepared, purified, and identified as Reference [16]. CD133$^+$ Huh-7 cells were transfected with pHRE-Egrl-HSV-TK by PEI-FePt-NPs as the above, and then incubated in 5% CO_2 at 37°C. Two days later, the transfected cells were diluted into 3×10^5/ml single cell suspension and seeded in 5 culture flasks (3 ml/flask). The grouping was as follows: (1) negative control group (untransfected), (2) ^{131}I-antiCD133McAb group (untransfected, radioimmunotherapy group), (3) magnetic hyperthermia group (untransfected, MFH group), (4) pHRE-Egrl-HSV-TK/GCV/^{131}I/anti-CD133McAb group (pHRE-Egrl-HSV-TK/^{131}I-anti-CD133McAb group), and (5) pHRE-Egrl-HSV-TK/GCV/^{131}I/anti-CD133McAb/MFH group (pHRE-Egrl-HSV-TK/^{131}I-anti-CD133McAb/MFH group). DMEM, ^{131}I-anti-CD133McAb (ultimate concentration: 50 μCi), and GCV (ultimate concentration: 5 μg/ml) were added to the corresponding group. After incubation for 24 h, PEI-FePt-NPs (ultimate concentration: 1 g/l) were added to the MFH group and pHRE-Egrl-HSV-TK/^{131}I-anti-CD133McAb/MFH group. The groups involved in MFH were placed on a flat coil of high-frequency magnetic induction heater (SPG-10A-II) with 215 kHz, 2.4 kW, and output current of 35 A for 1 h. The PHRE-Egrl-HSV-TK/^{131}I-anti-CD133McAb and pHRE-Egrl-HSV-TK/^{131}I-anti-CD133McAb/MFH groups were cultured in a hypoxic environment at 37°C for 2 days, and the other groups were cultured in 5% CO_2 at 37°C for 2 days.

2.6.1. The Examination of the Cell Proliferation Inhibitory Rate of Each Group. Some cells of each group were taken out to prepare single cell suspension, respectively, and then seeded in 96-well plates (200 μl/well), and 5 replicate wells were set in each group. After incubation for 24 h, each well was added with 20 μl MTT, and then continued to incubate. 4 h later, the medium in each well was discarded, and then, DMSO was added (150 μl/well). After shaking for 10 min, OD values at 493 nm were examined by a microplate reader. Cell proliferation inhibitory rate = $(1 - (\text{OD of experimental group} - \text{OD of blank control group})/(\text{OD of negative control group} - \text{OD of blank control group})) \times 100\%$.

2.6.2. The Detection of Cell Apoptosis of Each Group. The remaining cells of each group above were collected and washed with cold PBS 3 times. After centrifugation, the supernatant was discarded, and the cells were suspended in an annexin-binding buffer. Then, Annexin V and PI were added, respectively. After reaction at room temperature in dark for 15 min, the annexin-binding buffer was added, and the cell apoptosis rate of each group was analyzed by flow cytometry within 1 h.

2.7. The Analysis of VEGF and CD44 Protein Expression. After treatment for 24 h as Section 2.6, LCSCs were collected, and then, VEGF and CD44 protein of each group were detected by western blot, respectively.

2.8. Statistical Analysis. All data used in the experiments were expressed as mean ± SD. Statistical analysis was performed using SPSS 20.0 software. One-way analysis of variance was used. ANOVA or t test was used for comparison. $p < 0.05$ was considered statistically significant.

3. Results

3.1. Sorting, Identification, and Culture of CD133+ Huh-7 Cells. Flow cytometry analysis showed that the CD133 expression rate of Huh-7 cells was 9.61% (Figure 1(a)), and then, CD133$^+$ Huh-7 cells were sorted by flow cytometry and seeded in serum-free DMEM/F12 medium with cell growth factors. Six days later, a few small cell spheres appeared in the medium (Figure 1(b)). On the 13th day, many big cell spheres were suspended in the medium (Figures 1(c)–1(e)). Figure 1(d) is a cluster of CD133$^+$ Huh-7 cells in an unstained bright field, and Figure 1(e) shows the clusters of CD133$^+$ Huh-7 cells cloned with soft agar. These data indicate that the sorted liver cancer CD133$^+$ Huh-7 cells have a strong clonality.

3.2. Characterization of FePt-NPs. Figure 2(a) is an XRD pattern of the prepared FePt-NPs, with sharp diffraction peaks. The interplanar spacing (d value) corresponding to each diffraction peak corresponded to the Powder Diffraction Standards Association Card (JCPDS: 43-1359), indicating FePt-NPs prepared were in crystalline state. TEM examination showed that FePt-NPs were about 3 ± 1 nm in size, with good dispersion (Figure 2(b)).

The magnetic fluid of FePt-NPs and PEI-FePt-NPs was placed at 4°C, respectively. 24 h later, the FePt-NP magnetic fluid showed a clear sedimentation layer with clear boundary. The upper layer was colorless and translucent, and the lower layer was black. By comparison, the PEI-FePt-NP magnetic fluid showed mild sedimentation after one week and homogeneously dispersed again after shaking. This indicates that PEI modification improved the suspension stability of FePt-NPs.

3.3. Magnetothermal Effect of FePt-NPs and PEI-FePt-NPs. Figure 3 shows the magnetothermal effects of FePt-NPs and PEI-FePt-NPs at different concentrations and different magnetic field intensities. When magnetic field intensity was constant, the temperature of four concentrated magnetic fluids increased with time. The larger the magnetic fluid concentration, the stronger the heating ability (Figures 3(a) and 3(b)). When the concentration of the magnetic fluid was constant, the temperature of the magnetic fluid increased under the four magnetic field strengths with time. The higher the magnetic field strength, the stronger the temperature rising ability (Figures 3(c) and 3(d)). Either the same concentration or the same magnetic field intensity, the magnetic fluid of FePt-NPs and PEI-FePt-NPs both warmed up fast within the first 20 minutes and then slowly remained at a certain temperature range. The results suggested that FePt-NPs and PEI-FePt-NPs had good heating performance in AMF and may be used for magnetic fluid hyperthermia.

3.4. Identification of Eukaryotic Expression Plasmids pHRE-Egr1-HSV-TK

3.4.1. Enzyme Digestion Identification. pEgr1-HSV-TK and pHRE-Egr1p-HSV-TK were identified by restriction enzyme

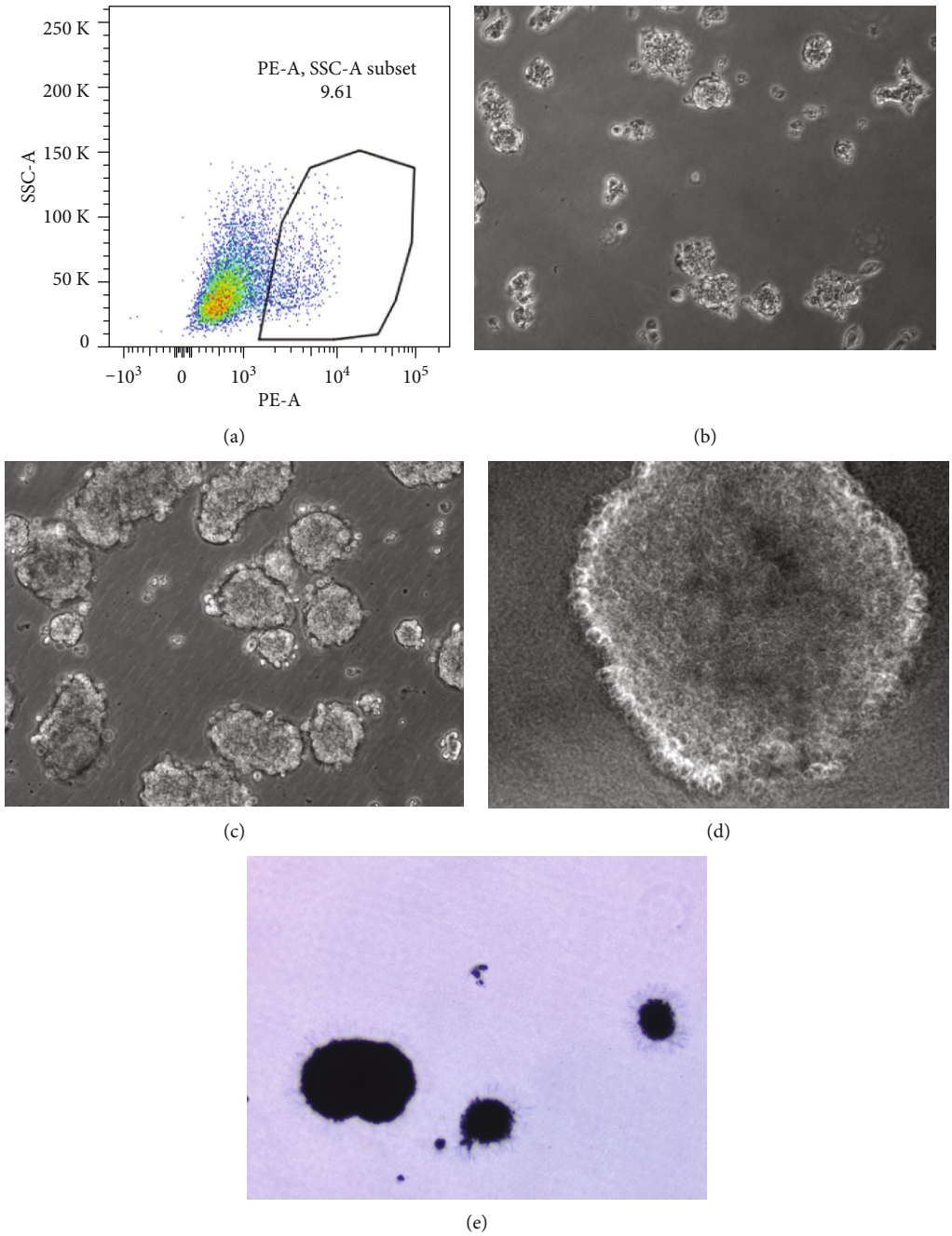

Figure 1: Identification and cloned spheres of CD133$^+$ Huh-7 cells. (a) 9.61% CD133 expression rate of Huh-7 cells tested by flow cytometry. (b) Cloned spheres of CD133$^+$ Huh-7 cells cultured for 6 days. (c) Cloned spheres of CD133$^+$ Huh-7 cells cultured for 13 days. (d) CD133$^+$ Huh-7 cell cluster photographed in an unstained bright field. (e) CD133$^+$ Huh-7 cell clusters photographed after cloning with soft agar.

digestion, respectively. As shown in Figure 4(a), there was a small band of about 2500 bp and a large band of about 4500 bp after pEgr1-HSV-TK was digested. By comparison, there was a small band of about 400 bp between 250 bp and 500 bp bands after pHRE-Egr1-HSV-TK was digested (Figure 4(b)). It was indicated that the 5HRE fragment was successfully inserted into pEgr1-HSV-TK.

3.4.2. Sequencing Identification. Figure 4(c) is a sequencing map of pHRE-Egr1-HSV-TK. Compared with the canonical sequence of 5HRE-Egr1p, the sequence examined of pHRE-Egr1-HSV-TK was completely correct, indicating that the 5HRE-Egr1p fragment was successfully inserted, and pHRE-Egr1-HSV-TK was successfully constructed.

3.5. Gene Transfection Using PEI-FePt-NPs Used as a Carrier In Vitro

3.5.1. Experiment of DNA Binding to PEI-FePt-NPs. Figure 5(a) is an agarose gel electrophoresis map of DNA

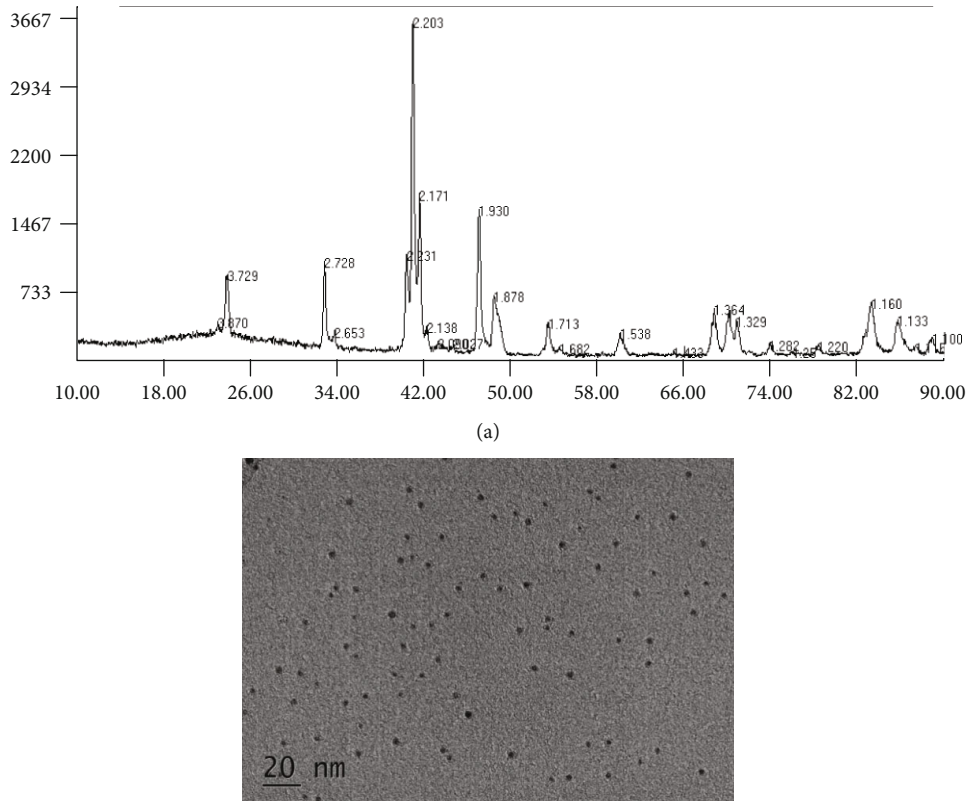

Figure 2: Characterization of iron-platinum nanoparticles. (a) XRD pattern of FePt-NPs. (b) TEM of FePt-NPs.

binding to PEI-FePt-NPs. It can be seen that when the mass ratio of pHRE-Egr1-HSV-TK and PEI-FePt-NPs was 1 : 40, all plasmids could bind to PEI-FePt-NPs. 1 : 40 (mass ratio) was thus considered the optimum ratio of DNA and PEI-FePt-NPs to bind.

3.5.2. DNA Protection from DNase1 Digestion by PEI-FePt-NPs. Figure 5(b) is an experimental electrophoresis of DNase1 digestion protection of PEI-FePt-NPs/DNA. It can be seen that PEI-FePt-NPs/pHRE-Egr1-HSV-TK remained stable after DNase1 digestion within 60 minutes, whereas the naked plasmids were almost completely digested at 1 min, with no bands observed, indicating that PEI-FePt-NPs could effectively protect the plasmids from DNase1 digestion.

3.5.3. DNA Release from PEI-FePt-NPs/DNA Complex. Figure 5(c) is an experimental gel electrophoresis of DNA release from the PEI-FePt-NPs/pHRE-Egr1-HSV-TK complex. Within 3 days, released DNA gradually increased, and there was almost no difference after the fourth day and the fifth day, indicating that DNA could effectively release from the complex (PEI-FePt-NPs/pHRE-Egr1-HSV-TK) in appropriate conditions.

3.5.4. PEI-FePt-NP Gene Transfection Efficiency. pHRE-Egrl-EGFP were transfected into $CD133^+$ Huh-7 cells by PEI-FePt-NPs, and the transfection efficiency was 53.65 ± 3.40%, significantly higher than 38.76 ± 4.50% transfection by lipofection, a common transfection reagent ($p < 0.05$), indicating that PEI-FePt-NPs can be served as vectors for gene transfer (Table 1).

3.6. Radioactivity Detection of ^{131}I-Anti-CD133McAb. ^{131}I was labeled to anti-CD133McAb, and the crude product of anti-CD133McAb labeled with ^{131}I was purified by PD10 column to remove free ^{131}I. Figure 6(a) is a TLC quality control chart of pure ^{131}I-anti-CD133McAb, and Table 2 is quality control peak area % report form of pure ^{131}I-CD133McAb TLC. The radiochemical purity of anti-CD133McAb labeled with ^{131}I was 100%, and the labeling rate was 36%.

After being placed at room temperature for 6 h, the radiochemical purity of ^{131}I-anti-CD133McAb was still 100% by TLC (Figure 6(b) and Table 3), indicating that ^{131}I-anti-CD133McAb prepared had good radiation stability.

3.7. Liver Cancer Stem Cells Were Intervened by pHRE-Egrl-HSV-TK/^{131}I-Anti-CD133McAb/MFH In Vitro

3.7.1. Cell Proliferation Inhibition and Apoptosis. Cell proliferation inhibition was tested by MTT, and cell apoptosis was examined by flow cytometry. As shown in Table 4 and Figure 7(a), PEI-FePt-NP-mediated radiation-gene therapy combined with magnetic fluid hyperthermia greatly inhibited LCSC proliferation and induced cell apoptosis. The cell

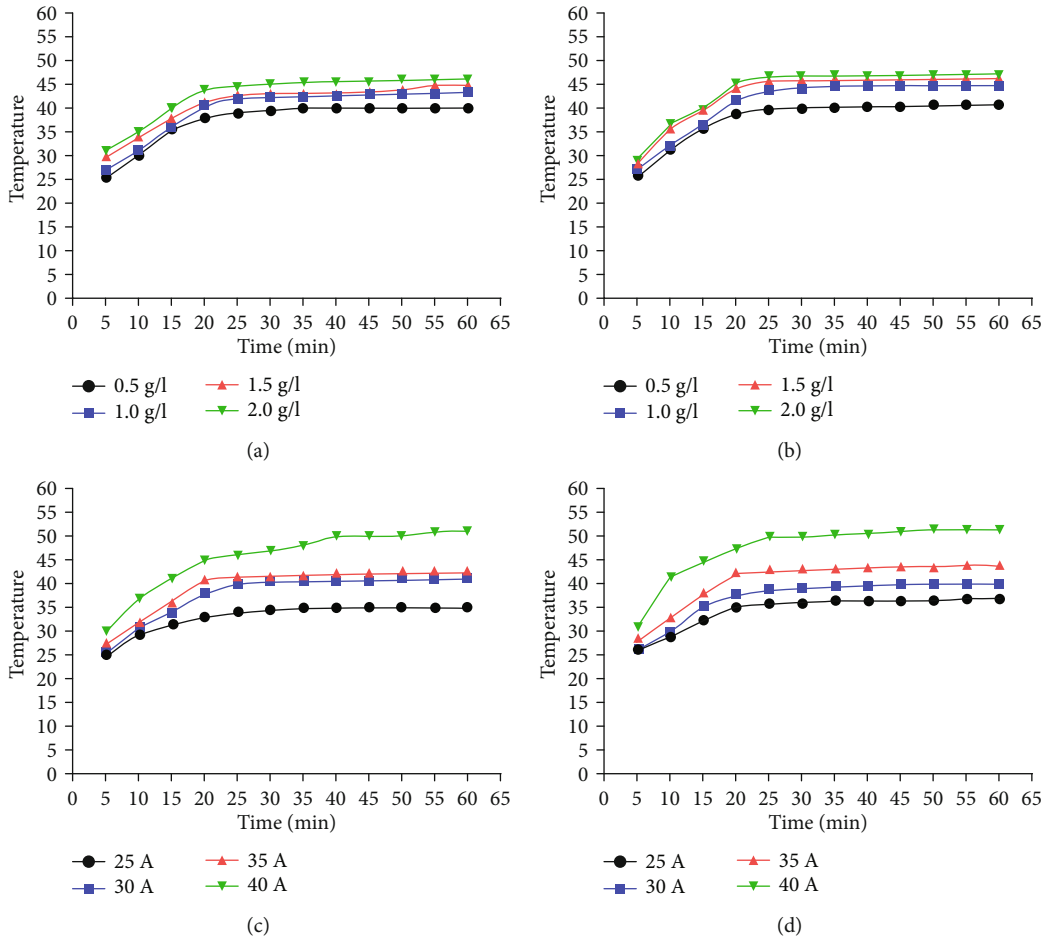

Figure 3: *In vitro* magnetic induction heating curves of FePt-NPs and PEI-FePt-NPs. (a) Magnetic induction heating curves of FePt-NPs with different concentrations. (b) Magnetic induction heating curves of PEI-FePt-NPs with different concentrations. (c) Magnetic induction heating curves of FePt-NPs under different magnetic field strengths. (d) Magnetic induction heating curves of PEI-FePt-NPs under different magnetic field strengths.

proliferation inhibition rate and apoptosis rate of the pHRE-Egrl-HSV-TK/^{131}I-anti-CD133McAb/MFH group was up to 63% and 49.22%, respectively, both significantly higher than those of any other groups ($p < 0.05$).

3.7.2. Expression of VEGF and CD44 Proteins. Figure 7(b) shows VEGF and CD44 protein expression in LCSCs by western blot. VEGF and CD44 proteins of the pHRE-Egrl-HSV-TK/^{131}I-anti-CD133McAb/MFH group both clearly decreased. Figure 7(c) displays the protein expression levels of VEGF and CD44 based on the β-actin gray value. Compared with the negative control group and all the other experimental groups, the expression levels of VEGF and CD44 proteins of the pHRE-Egrl-HSV-TK/^{131}I-anti-CD133McAb/MFH group were both reduced, and there was a statistically significant difference ($p < 0.001$). These data suggest that the combination of targeted radiation-gene therapy and magnetic fluid hyperthermia mediated by PEI-FePt-NPs significantly inhibited VEGF and CD44 protein expression in LCSCs.

4. Discussion

4.1. Preparation, Modification, and Characterization of FePt-NPs. Owing to the magnetic property at the nanometer scale, magnetic nanoparticles have been widely used in many fields, without the exception of the medical field, including magnetic resonance imaging systems, biological separation, immunoassays, and magnetic hyperthermia. They can be primarily classified into metals, metal oxides, and metal alloys. Among them, nanoiron oxides have been extensively exploited in tumor thermotherapy and imaging diagnosis because of their handy synthesis and good biocompatibility. As for metal alloy FePt-NPs, it has a strong magnetic property, excellent oxidation resistance [18], small superparamagnetic critical dimension, high magnetic energy level, high Curie temperature, and eximious biocompatibility [19–22], showing a promising application potential in the biomedicine field. Nowadays, chiefly prepared by mechanical condensation method [23], vacuum deposition method [24], magnetron sputtering method [25, 26], and some chemical methods, FePt-NPs were synthesized in this study by the

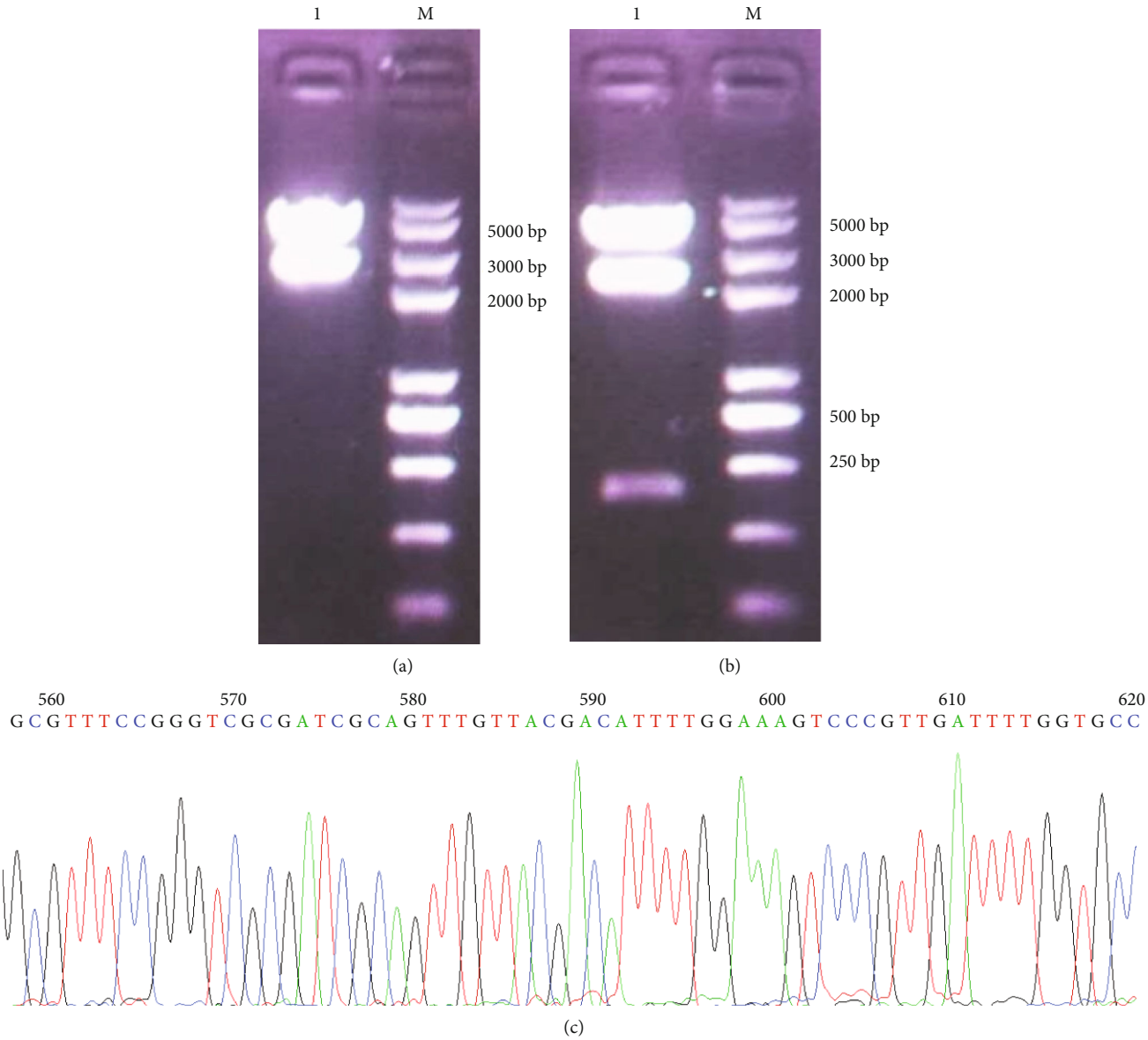

Figure 4: Identification of eukaryotic expression plasmids pHRE-Egr1-HSV-TK. (a) Enzyme identification map of pEgr1-HSV-TK (lane 1: pEgr1-HSV-TK digested with BglII+XhoI; lane M: marker). (b) Enzyme identification map of pHRE-Egr1-HSV-TK (lane 1: pHRE-Egr1-HSVTK digested with BglII+XhoI; lane M: marker). (c) Sequencing map of pHRE-Egr1p-HSV-TK.

inverse microemulsion method in combination with the azeotropic distillation device (Organic benzene was used as the continuous phase. The iron precursor, the iron nitrate platinum precursor, chloroplatinic acid, and sodium chloride aqueous solution were exploited as the dispersed phase, and cetyltrimethylammonium bromide was added as the surfactant). After removing the redundant water by distillation, we removed the free surfactant at high temperature. Finally, hydrogen reduction was adopted to get FePt-NPs. TEM detected that the FePt-NPs were about 3.0 nm in diameter, uniform in size with good dispersion, meeting the requirements for particle size in the biomedical field. Meanwhile, the crystalline FePt-NPs were confirmed by X-ray diffraction analysis [27].

Polyethylenimine (PEI) is a commonly used cationic surfactant. Owing to the strong ability to bind DNA and adhere to cells, PEI can be used as the surface modifier for many substances to increase their biocompatibility, dispersibility, and chemical stability, which is thus applied to the biological science field [28]. The principle is that PEI can effectively diminish the surface potential energy of the nanoparticles by electrostatic repulsion, or establish a material barrier near the particles to prevent them from getting close to each other to stabilize the system, thereby improving the particles' dispersibility and biocompatibility [29–31]. In the current study, FePt-NPs were modified by PEI and the results showed good suspension stability of PEI-FePt-NPs.

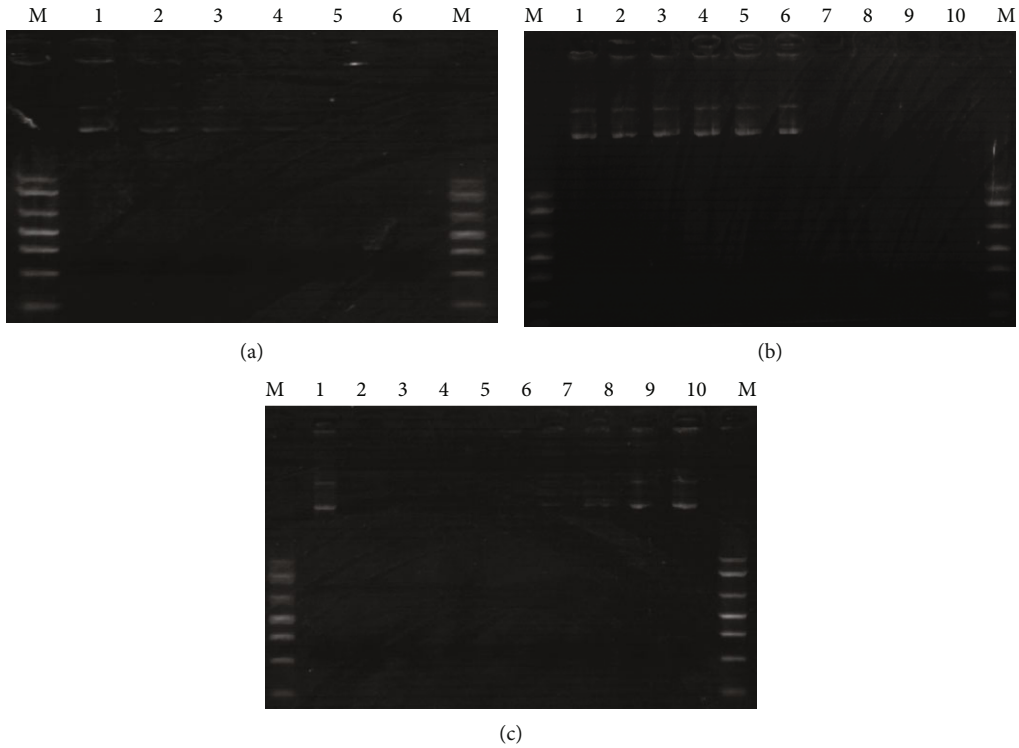

Figure 5: The potential investigation of PEI-FePt-NPs used as a carrier for gene transfection. (a) Electrophoresis of pHRE-Egr1-HSV-TK binding to PEI-FePt-NP (lane 1, 1 : 0 (100 ng plasmid DNA, no magnetic nanoparticles); lane 2, 1 : 5; lane 3, 1 : 10; lane 4, 1 : 20; lane 5, 1 : 40; lane 6, 1 : 80; and lane M: DNA marker (standard band from top to bottom is 2000 bp, 1500 bp, 1000 bp, 700 bp, 500 bp, 300 bp, and 100 bp)). (b) Electrophoresis map of DNase1 digestion protection of PEI-FePt-NPs/DNA (lane 1: 100 ng of nude pHRE-Egr1-HSV-TK; lane 2: complex digested for 1 min; lane 3: complex digested for 10 min; lane 4: complex digested for 30 min; lane 5: complex digested for 45 min; lane 6: complex digested for 1 h; lane 7: naked pHRE-Egr1-HSV-TK digested for 1 min; lane 8: naked pHRE-Egr1-HSV-TK digested for 10 min; lane 9: naked pHRE-Egr1-HSV-TK digested for 30 min; lane 10: naked pHRE-Egr1-HSV-TK digested for 45 min; and lane M: DNA marker (2000 bp, 1500 bp, 1000 bp, 700 bp, 500 bp, 300 bp, and 100 bp from top to bottom). (c) Electrophoresis map of DNA release from PEI-FePt-NPs/pHRE-Egr1-HSV-TK (lane 1: 100 ng pHRE-Egr1-HSV-TK; lane 2: 1 h; lane 3: 4 h; lane 4: 8 h; lane 5: 12 h; lane 6: 1 d; lane 7: 2 d; lane 8: 3 d; lane 9: 4 d; lane 10: 5 d; and lane M: DNA marker (2000 bp, 1500 bp, 1000 bp, 700 bp, 500 bp, 300 bp, and 100 bp from top to bottom)).

Table 1: Transfection efficiency of $CD133^+$ Huh-7 cells *in vitro*.

Group	Transfection efficiency (%)
PEI-FePt-NPs transfection	53.65 ± 3.40
Liposome transfection	38.76 ± 4.50

The PEI-FePt-NP group compared with liposome group, $p < 0.05$.

Under the action of AMF, ferromagnetic materials have thermogenesis because of postmagnetic effects, domain enthalpy resonance, hysteresis effect, and natural resonance. Magnetic fluid hyperthermia can control temperature within a desired range. In this study, FePt-NPs and PEI-FePt-NPs prepared by the reverse microemulsion method both had ideal magnetothermal effect in AMF. When the magnetic field strength was constant, the higher is the magnetic fluid concentration and the stronger is the heating ability. If the magnetic fluid concentration is invariable, the higher magnetic field strength indicates a stronger heating capacity. It is worth noting that the temperature rose fast in the first 20 minutes, and then slowly maintained at a certain level. In terms of 1 g/l FePt-NP and 1 g/l PEI-FePt-NP magnetic fluids, the temperature was maintained at 43°C or so, which was a desired temperature for tumor thermotherapy. The reason lies in that tumor cells are subjected to be damaged when the temperature is maintained at 39-45°C, with few or no damage to the surrounding normal cells and tissues. This data suggest that PEI-FePt-NPs may be used for magnetic fluid hyperthermia.

4.2. Construction of pHRE-Egr1-HSV-TK Eukaryotic Expression Plasmids. As a remedy by transferring the exogenous gene into target cells and using the expression products of the exogenous gene to treat disease, gene therapy can treat cancer by inducing tumor cells' apoptosis, activating body immune system and inhibiting tumor angiogenesis. With the rapid progress of molecular biology and genetic engineering technology, gene therapy for HCC has undergone fast growth. The gene therapies for HCC principally encompass suicide gene therapy, antisense gene therapy, tumor suppressor gene therapy, immune gene therapy, antineovascularization therapy, combined gene therapy, resistant gene therapy, and RNA interference. HSV-TK, a widely used suicide gene,

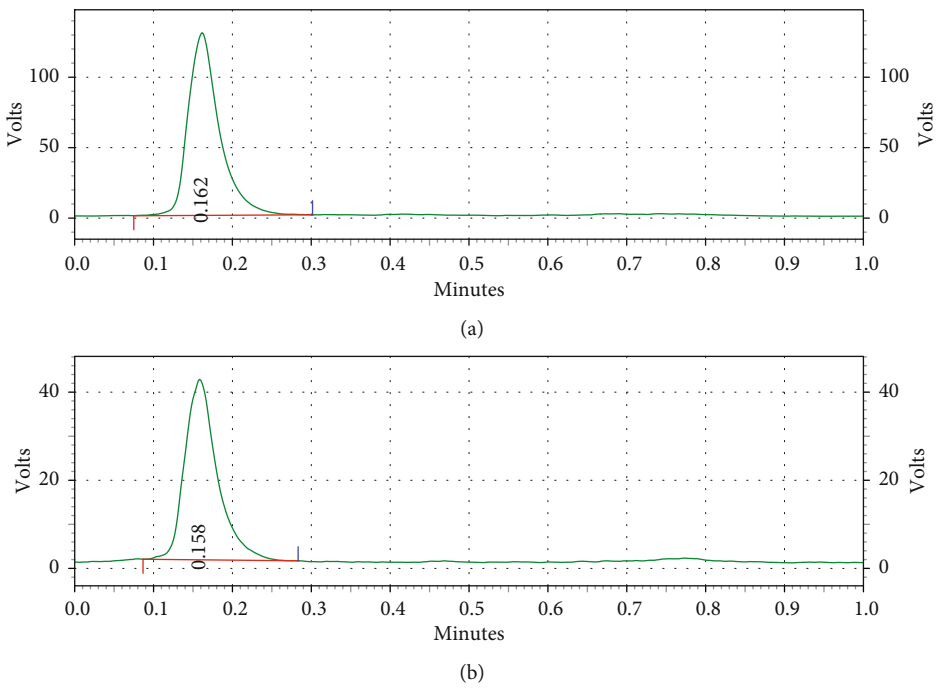

Figure 6: TLC quality control chart of ^{131}I labeled with anti-CD133McAb. (a). TLC quality control chart of ^{131}I-CD133McAb pure product. (b) TCL quality control chart after ^{131}I-anti-CD133McAb product was placed at room temperature for 6 h.

Table 2: ^{131}I-CD133 pure TLC quality control peak area % report form.

Retention time	Area	Area percentage (%)	Peak height	Percentage of height (%)
0.162	355656	100.000	129692	100.000
Total	355656	100.000	129692	100.000

Table 3: TCL control peak area % after ^{131}I-anti-CD133 placed at room temperature for 6 h.

Retention time	Area	Area percentage (%)	Peak height	Percentage of height (%)
0.158	117013	100.000	40969	100.000
Total	117013	100.000	40969	100.000

comes from herpes simplex virus and encodes thymidine kinase. The product HSV-TK expressed can concentrate in the tumor area to convert prodrug GCV into cytotoxic drug to selectively kill the tumor, thus reducing side effects [13]. But it is of extreme importance to select an appropriate regulatory sequence and activating mode to generate exact and efficient expression of the therapeutic gene. Egr-1 (early growth response gene 1, a radiation-inducing gene) promoter has some conserved domains that can feel physicochemical stimulation inside and outside to induce the corresponding gene to express itself, which has a good application prospect in gene therapy [32, 33]. When Egr-1 promoter is ligated into the upstream of cDNA, it can regulate the related gene expression in time and space by radiation [15]. As an anoxic sensitivity enhancer, HRE can mediate hypoxia and specifically bind up with the Egr-1 promoter to induce the downstream gene expression [14, 17]. We constructed pHRE-Egr1-HSV-TK, and the plasmids were confirmed correct by restriction enzyme digestion and sequencing in this study.

4.3. PEI-FePt-NPs Were Used as a Vector for Gene Transfection. The applicable gene delivery vector is another key to obtain the desired therapeutic effect. Although transfection efficiency of the viral vector system is high, its clinical application is strictly limited in consideration of security risks. While the nonviral vector system can avoid potential risks, its low transfection efficiency makes it difficult to obtain meaningful gene expression. Thus, how to break through the bottleneck of gene transfer has become a top priority in the gene therapy research field. With good potential in gene therapy, nanogene delivery is to encapsulate therapeutic genes, such as DNA and RNA, onto nanoparticles, which will then enter cells under the action of cell uptake to release the therapeutic molecules. If coupled with specific biomolecules, such as antibody, ligand, or aptamer, nanocarrier delivery is conducive to achieve targeted gene treatment for cancer and other diseases. Compared with traditional vectors, nanocarriers have many edges, including no immunogenicity, genotoxicity, and cytotoxicity, allowing genes to release slowly, improving transfection efficiency and bioavailability of transfection products, and obtaining long-term stable expression of transgenes [34–36]. It not only integrates the strength of viral vectors and conventional nonviral vectors but also averts the defects of both, thus having turned into a new carrier system with great application prospects. Currently, a variety of nanogene transfer vectors are being

Table 4: Results of MTT experiments after different methods of treatment.

Group	OD value	Proliferation inhibition rate (%)
Negative control group	1.322 ± 0.028	
^{131}I-anti-CD133McAb group	0.991 ± 0.019^{ab}	25
MFH group	0.945 ± 0.046^{ab}	29
pHRE-Egrl-HSV-TK/^{131}I-anti-CD133McAb group	0.795 ± 0.037^{ab}	40
pHRE-Egrl-HSV-TK/^{131}I-anti-CD133McAb/MFH group	0.488 ± 0.051^{a}	63

[a] Compared with the control group, $p < 0.05$; [b] compared with the combination treatment group, $p < 0.05$.

developed. As a sort of inorganic nonviral carrier [37, 38], magnetic nanocarriers are handy to prepare and surfacely modify, with good biocompatibility and no tissue cytotoxicity. Besides the characteristics of general nanoparticles, it has superparamagnetism and can thus directionally migrate in AMF to realize gene-targeted therapy [39]. Furthermore, given that magnetic nanoparticles also can be induced to warm, they thus may be used for tumor thermotherapy in AMF [15].

In this study, PEI-FePt-NPs were combined with DNA (using pHRE-Egr1-EGFP as a model) to prepare composite nanoparticles. Biological characteristic detection experiments confirmed that the optimal ratio of DNA binding to PEI-FePt-NPs was 1 : 40 (the mass ratio); the plasmids in the composite nanoparticles could be protected from Dnase1 enzyme digestion and could slowly release from the complex under certain conditions. The recombinant pHRE-Egr1-EGFP was transfected into CD133$^+$ Huh-7 cells by PEI-FePt-NPs, the transfection efficiency of which was $53.65 \pm 3.40\%$ in line with flow cytometry analysis. These results indicate that PEI-FePt-NPs may be used as the vector for gene transfer.

4.4. Preparation, Purification, and Identification of ^{131}I-Anti-CD133McAb. Tumor radioimmunotherapy is a strategy to combine radionuclide with the tumor-specific monoclonal antibody to seek a targeted treatment for cancer, allowing target cells to be exposed with more radiation, while with less damage to the surrounding normal tissues and cells. In 1978, Golden et al. successfully applied radioimmunotherapy to tumor imaging and therapy study. The CD133 antigen, a specific molecule marker independently expressed on the surface of various tumor stem cells, is bound up with tumor self-renewal, differentiation potential, radiochemotherapy resistance, recurrence, and prognosis [9, 40–42]. The killing effect of paclitaxel nanoparticles labeled with anti-CD133McAb on breast cancer stem cells was remarkably better than that of free paclitaxel [43]. Anti-CD133McAb-directed toxins have also achieved good therapeutic effects on ovarian cancer stem cells [44]. In liver cancer tissues, the positive rate of CD133 antigen was 76.3%, and some researchers have utilized the CD133 antibody to separate liver cancer stem cells from liver cancer tissues and liver cancer cell lines [45, 46]. CD133 antigen is expected to be a new target for liver cancer stem cell treatment. ^{131}I with 8.05-day physical half-life can emit both gamma and beta rays. The latter (β) can be used for tumor treatment, and the former (γ) for medical imaging. Numerous clinical practices have shown that the human body has good tolerance to ^{131}I, with few adverse effects. Anti-CD133McAb labeled with ^{131}I can selectively concentrate in the tumor region, and it can improve the targeting of ^{131}I and HSV-TK for LCSCs treatment. In this study, ^{131}I-anti-CD133McAb prepared by the chloramine T method was purified by the PD10 column, with 100% of radiochemical purity and 36% of the labeling rate. After 6 h at room temperature, the radiochemical purity was still 100%, showing excellent radiological stability.

4.5. Targeted Intervention of pHRE-Egr1-HSV-TK/^{131}I-Anti-CD133McAb/MFH for LCSCs In Vitro. LCSCs are to blame in the process of occurrence, progress, metastasis, and recurrence of HCC and responsible for the failure of HCC treatment. Therefore, a successful HCC treatment should aim for LCSCs, without an exception of nonstem cells differentiated from LCSCs. As the specific molecule marker independently expressed on the surface of various tumor stem cells, the CD133 antigen is closely involved in tumor self-renewal, differentiation potential, radiochemotherapy resistance, recurrence, and prognosis [47, 48], possibly becoming a new target for cancer stem cell treatment.

The expression rate of CD133 antigen in Huh-7 cell line was 9.61%, and CD133$^+$ Huh-7 cells were sorted by flow cytometry in the present study. With serum-free culture, the screened CD133$^+$ Huh-7 cells successfully formed into cloned spheres or clusters, indicating that LCSCs with cloning ability have been successfully sorted out. We combined anti-CD133McAb labeled with ^{131}I, pHRE-Egr1-HSV-TK, and MFH together to intervene with LCSCs by using PEI-FePt-NPs as a linker. The results showed that radiation-gene therapy combined with MFH prominently inhibited LCSC proliferation and induced cell apoptosis, significantly better than any of the individual interventions.

As one of the pivotal angiogenesis regulators, VEGF is overexpressed in HCC tissues, playing a vital role in the growth and metastasis of liver cancer [49]. CD44, the hyaluronic acid receptor that functions in tissue remodeling, cell matrix adhesion, and cell migration, has been recognized as one of critical biomarkers for multiple solid tumor stem cells [50]. Yang et al. [51] reported that CD44$^+$ liver cancer cells exhibited more aggressiveness than CD44$^-$ liver cancer cells did. In this study, western blot analysis showed that VEGF and CD44 proteins both dwindled at different levels in each experimental group. Notably, they decreased most significantly in the pHRE-Egr1-HSV-TK/^{131}I-anti-CD133McAb/MFH group, indicating that radiation-gene therapy in combination with

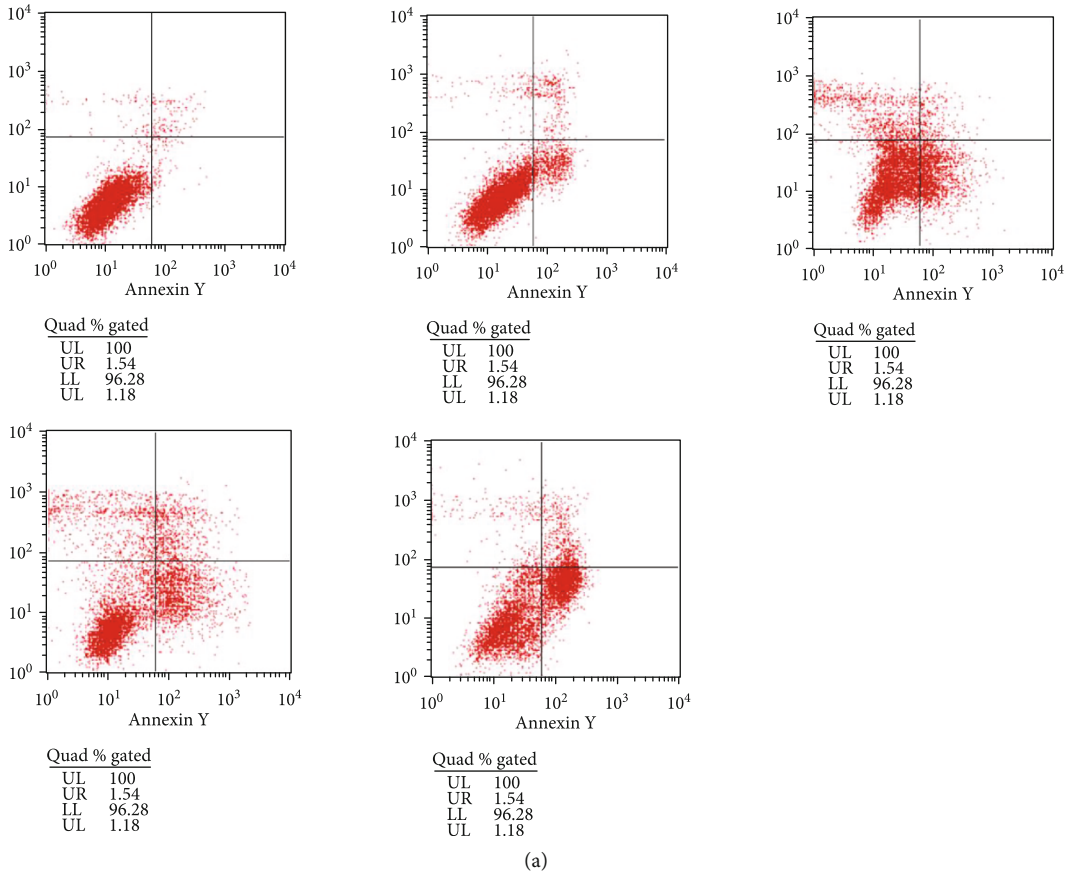

Figure 7: Cell apoptosis and related proteins' protein expression of each group after treatment. (a) Cell apoptosis analyzed by flow cytometry. (1) Negative control group. (2) ^{131}I-anti-CD133McAb group. (3) MFH group. (4) pHRE-Egrl-HSV-TK/^{131}I-anti-CD133McAb group. (5) pHRE-Egrl-HSV-TK/^{131}I-anti-CD133McAb/MFH group. (b) Expression of VEGF and CD44 proteins after treatment tested by western blot. (1) Negative control group. (2) ^{131}I-anti-CD133McAb group. (3) MFH group. (4) pHRE-Egrl-HSV-TK/^{131}I-anti-CD133McAb group. (5) pHRE-Egrl-HSV-TK/^{131}I-anti-CD133McAb/MFH group). (c) Expression level of VEGF and CD44 proteins based on the β-actin gray value and analyzed by an image processing system. (1) Negative control group. (2) ^{131}I-anti-CD133McAb group. (3) MFH group. (4) pHRE-Egrl-HSV-TK/^{131}I-anti-CD133McAb group. (5) pHRE-Egrl-HSV-TK/131I-anti-CD133McAb/MFH group).

magnetic fluid hyperthermia may exert an antitumor effect by inhibiting angiogenesis, proliferation, and invasion through restraining the expression of VEGF and CD44 proteins.

In summary, LCSCs ($CD133^+$) were separated from the Huh-7 cell line by flow cytometry and constructed recombinant plasmids pHRE-Egr1-HSV-TK in the present study. Using PEI-FePt-NPs as the vector, LCSCs were transfected with pHRE-Egr1-HSV-TK, with good transfection effect. Besides, ^{131}I-anti-CD133McAb was successfully prepared, with 100% radiochemical purity, 36% labeling rate, and good radioactive stability. Targeted radiation-gene therapy combined with magnetic fluid hyperthermia mediated by PEI-FePt-NPs (pHRE-Egr1-HSV-TK/^{131}I-anti-CD133McAb/MFH) could efficaciously inhibit LCSC proliferation and induce cell apoptosis. The mechanism may be related to the downregulation of VEGF and CD44 protein expression, thereby restraining tumor angiogenesis, tumor stem cell proliferation, and invasion. This study offers a theoretical and practicable approach for LCSC treatment but is simply limited to experiments *in vitro*. Animal experiments *in vivo* and the therapeutic mechanism are currently ongoing.

Data Availability

The graphics and quantitative data used to support the findings of this study are included within the article.

Conflicts of Interest

The authors declare that they have no conflicts of interest.

Authors' Contributions

Mei Lin conceived and designed the study, performed some experiments, analyzed the data, and wrote the manuscript. Yanhong Xiao conceived and performed some experiments, analyzed some data, and contributed to the manuscript writing. Xingmao Jiang and Jun Zhang gave some constructive guidance, performed some experiments and contributed to some data analysis. Ting Guo and Yujuan Shi performed some experiments and contributed to some data analysis. All authors reviewed the manuscript. Mei Lin and Yanhong Xiao contributed equally.

Acknowledgments

The work is financially supported by the National Natural Science Foundation of China (81571797), Natural Science Foundation of Jiangsu, China (BK20151352), and Taizhou People's Hospital Medical Innovation Team Foundation, China (CXTDA201901).

References

[1] K. J. Lafaro, A. N. Demirjian, and T. M. Pawlik, "Epidemiology of hepatocellular carcinoma," *Surgical Oncology Clinics of North America*, vol. 24, no. 1, pp. 1–17, 2015.

[2] J. Balogh, D. I. Victor, E. H. Asham et al., "Hepatocellular carcinoma: a review," *Journal of Hepatocellular Carcinoma*, vol. 3, pp. 41–53, 2016.

[3] M. Najafi, B. Farhood, and K. Mortezaee, "Cancer stem cells (CSCs) in cancer progression and therapy," *Journal of Cellular Physiology*, vol. 234, no. 6, pp. 8381–8395, 2019.

[4] F. Collina, M. di Bonito, V. Li Bergolis et al., "Prognostic value of cancer stem cells markers in triple-negative breast cancer," *BioMed Research International*, vol. 2015, Article ID 158682, 10 pages, 2015.

[5] F. de Sousa e Melo, A. V. Kurtova, J. M. Harnoss et al., "A distinct role for $Lgr5^+$ stem cells in primary and metastatic colon cancer," *Nature*, vol. 543, no. 7647, pp. 676–680, 2017.

[6] T. Oikawa, "Cancer stem cells and their cellular origins in primary liver and biliary tract cancers," *Hepatology*, vol. 64, no. 2, pp. 645–651, 2016.

[7] G. Castelli, E. Pelosi, and U. Testa, "Liver Cancer: molecular characterization, clonal evolution and Cancer stem cells," *Cancers*, vol. 9, no. 12, p. 127, 2017.

[8] L. MacDonagh, S. G. Gray, E. Breen et al., "Lung cancer stem cells: the root of resistance," *Cancer Letters*, vol. 372, no. 2, pp. 147–156, 2016.

[9] A. Nomura, S. Banerjee, R. Chugh et al., "CD133 initiates tumors, induces epithelial-mesenchymal transition and increases metastasis in pancreatic cancer," *Oncotarget*, vol. 6, no. 10, pp. 8313–8322, 2015.

[10] M. Gao, Y. Kong, G. Yang, L. Gao, and J. Shi, "Multiple myeloma cancer stem cells," *Oncotarget*, vol. 7, no. 23, pp. 35466–35477, 2016.

[11] A. Suetsugu, M. Nagaki, H. Aoki, T. Motohashi, T. Kunisada, and H. Moriwaki, "Characterization of $CD133^+$ hepatocellular carcinoma cells as cancer stem/progenitor cells," *Biochemical and Biophysical Research Communications*, vol. 351, no. 4, pp. 820–824, 2006.

[12] A. Jordan, P. Wust, R. Scholz et al., "Cellular uptake of magnetic fluid particles and their effects on human adenocarcinoma cells exposed to AC magnetic fields in vitro," *International Journal of Hyperthermia*, vol. 12, no. 6, pp. 705–722, 1996.

[13] Q. Tang, D. Chen, M. Lu, and P. Liu, "Combination of PEI-$Mn_{0.5}Zn_{0.5}Fe_2O_4$ nanoparticles and pHsp 70-*HSV-TK*/GCV with magnet-induced heating for treatment of hepatoma," *International Journal of Nanomedicine*, vol. 10, pp. 7129–7143, 2015.

[14] M. Lin, D. Zhang, J. Huang et al., "An evaluation on transfection efficiency of pHRE-Egr1-EGFP in hepatocellular carcinoma cells Bel-7402 mediated by PEI-MZF-NPs," *Journal of Nanomaterials*, vol. 2011, Article ID 136052, 10 pages, 2011.

[15] M. Lin, J. Huang, J. Zhang et al., "The therapeutic effect of PEI-$Mn_{0.5}Zn_{0.5}Fe_2O_4$ nanoparticles/pEgr1-HSV-TK/GCV associated with radiation and magnet-induced heating on hepatoma," *Nanoscale*, vol. 5, no. 3, pp. 991–1000, 2013.

[16] M. Lin, J. Huang, X. Jiang et al., "A combination hepatoma-targeted therapy based on nanotechnology: pHRE- Egr1-HSV-TK/^{131}I-antiAFPMcAb-GCV/MFH," *Scientific Reports*, vol. 6, no. 1, 2016.

[17] J. Zhang, K. Guo, and S. Chai, "Cell-killing effect of MAR regulating HSV-tk/GCV suicide gene system on ECA109 cells," *International Journal of Clinical and Experimental Pathology*, vol. 10, pp. 817–822, 2017.

[18] D. Ho, X. Sun, and S. Sun, "Monodisperse magnetic nanoparticles for theranostic applications," *Accounts of Chemical Research*, vol. 44, no. 10, pp. 875–882, 2011.

[19] R.-J. Chung, K. L. Ou, S. P. Chen, and H. L. Liu, "Preparation of ICG-FePt nanoparticles promising for magnetic resonance imaging contrast agent and hyperthermia applications," *Advanced Powder Technology*, vol. 27, no. 3, pp. 994–999, 2016.

[20] P. Srinoi, Y. T. Chen, V. Vittur, M. Marquez, and T. Lee, "Bimetallic nanoparticles: enhanced magnetic and optical properties for emerging biological applications," *Applied Sciences*, vol. 8, no. 7, article 1106, 2018.

[21] S. Majidi, F. Zeinali Sehrig, M. Samiei et al., "Magnetic nanoparticles: applications in gene delivery and gene therapy," *Artificial Cells, Nanomedicine, and Biotechnology*, vol. 44, pp. 1–8, 2016.

[22] C. Lin, W. Li, S. Huang, C. S. Yeh, and C. M. Yang, "Hollow mesoporous silica nanosphere-supported FePt nanoparticles for potential theranostic applications," *Journal of Materials Chemistry B*, vol. 5, no. 36, pp. 7598–7607, 2017.

[23] N. H. Hai, N. M. Dempsey, M. Veron, M. Verdier, and D. Givord, "An original route for the preparation of hard FePt," *Journal of Magnetism and Magnetic Materials*, vol. 257, no. 2-3, pp. 139–145, 2003.

[24] M. Yu, H. Ohguchi, A. Zambano et al., "Orientation and magnetic properties of FePt and CoPt films grown on MgO(1 1 0) single-crystal substrate by electron-beam coevaporation," *Materials Science and Engineering B*, vol. 142, no. 2-3, pp. 139–143, 2007.

[25] N. Poudyal, K. H. Gandha, J. Liu, K. E. Elkins, H. Arami, and J. P. Liu, "Ferromagnetic FePt/Au core/shell nanoparticles prepared by solvothermal annealing," *IEEE Magnetics Letters*, vol. 7, pp. 1–5, 2016.

[26] L. Wu, A. Mendoza-Garcia, Q. Li, and S. Sun, "Organic phase syntheses of magnetic nanoparticles and their applications," *Chemical Reviews*, vol. 116, no. 18, pp. 10473–10512, 2016.

[27] S.-W. Chou, Y. H. Shau, P. C. Wu, Y. S. Yang, D. B. Shieh, and C. C. Chen, "In vitro and in vivo studies of fept nanoparticles for dual modal CT/MRI molecular imaging," *Journal of the American Chemical Society*, vol. 132, no. 38, pp. 13270–13278, 2010.

[28] O. S. Muddineti, B. Ghosh, and S. Biswas, "Current trends in using polymer coated gold nanoparticles for cancer therapy," *International Journal of Pharmaceutics*, vol. 484, no. 1-2, pp. 252–267, 2015.

[29] Y. Meng, S. Wang, C. Li et al., "Photothermal combined gene therapy achieved by polyethyleneimine-grafted oxidized mesoporous carbon nanospheres," *Biomaterials*, vol. 100, pp. 134–142, 2016.

[30] C. Liu, Y. Yu, L. Miao, Y. Liu, and W. Sun, "A comparative study of transfection of rat mesenchymal stem cells using polyethyleneimine-coated magnetic ferro-ferric oxide nanoparticles and lipofectamine," *International Journal of Clinical and Experimental Medicine*, vol. 9, pp. 6062–6069, 2016.

[31] M. Khoobi, S. F. Motevalizadeh, Z. Asadgol, H. Forootanfar, A. Shafiee, and M. A. Faramarzi, "Polyethyleneimine-modified superparamagnetic Fe_3O_4 nanoparticles for lipase immobilization: characterization and application," *Materials Chemistry and Physics*, vol. 149-150, pp. 77–86, 2015.

[32] W.-X. Peng, Y. Y. Wan, A. H. Gong et al., "Egr-1 regulates irradiation-induced autophagy through Atg4B to promote radioresistance in hepatocellular carcinoma cells," *Oncogenesis*, vol. 6, no. 1, article e292, 2017.

[33] J. Tang, X. Wang, Y. Xu, Y. Shi, Z. Liu, and Y. Yang, "Sodium-iodine symporter gene expression controlled by the EGR-1 Promoter," *Technology in Cancer Research & Treatment*, vol. 14, no. 1, pp. 61–69, 2015.

[34] H. Xu, Z. Li, and J. Si, "Nanocarriers in gene therapy: a review," *Journal of Biomedical Nanotechnology*, vol. 10, no. 12, pp. 3483–3507, 2014.

[35] G. Liu, M. Swierczewska, S. Lee, and X. Chen, "Functional nanoparticles for molecular imaging guided gene delivery," *Nano Today*, vol. 5, no. 6, pp. 524–539, 2010.

[36] K. Wang, F. M. Kievit, and M. Zhang, "Nanoparticles for cancer gene therapy: recent advances, challenges, and strategies," *Pharmacological Research*, vol. 114, pp. 56–66, 2016.

[37] O. Madkhali, G. Mekhail, and S. D. Wettig, "Modified gelatin nanoparticles for gene delivery," *International Journal of Pharmaceutics*, vol. 554, pp. 224–234, 2019.

[38] A. Amani, T. Kabiri, S. Shafiee, and A. Hamidi, "Preparation and characterization of PLA-PEG-PLA/PEI/DNA nanoparticles for improvement of transfection efficiency and controlled release of DNA in gene delivery systems," *Iranian Journal of Pharmaceutical Research*, vol. 18, no. 1, pp. 125–141, 2019.

[39] M. Czugala, O. Mykhaylyk, P. Böhler et al., "Efficient and safe gene delivery to human corneal endothelium using magnetic nanoparticles," *Nanomedicine*, vol. 11, no. 14, pp. 1787–1800, 2016.

[40] J. Jang, Y. Song, S. Kim, J. Kim, and H. R. Seo, "Potential mechanisms of CD133 in cancer stem cells," *Life Sciences*, vol. 184, pp. 25–29, 2017.

[41] G.-Y. Liou, "CD133 as a regulator of cancer metastasis through the cancer stem cells," *The International Journal of Biochemistry & Cell Biology*, vol. 106, pp. 1–7, 2019.

[42] C. Joseph, M. Arshad, S. Kurozomi et al., "Overexpression of the cancer stem cell marker CD133 confers a poor prognosis in invasive breast cancer," *Breast Cancer Research and Treatment*, vol. 174, no. 2, pp. 387–399, 2019.

[43] S. K. Swaminathan, E. Roger, U. Toti, L. Niu, J. R. Ohlfest, and J. Panyam, "CD133-targeted paclitaxel delivery inhibits local tumor recurrence in a mouse model of breast cancer," *Journal of Controlled Release*, vol. 171, no. 3, pp. 280–287, 2013.

[44] A. P. Skubitz, E. P. Taras, K. L. Boylan et al., "Targeting CD133 in an in vivo ovarian cancer model reduces ovarian cancer progression," *Gynecologic Oncology*, vol. 130, no. 3, pp. 579–587, 2013.

[45] A. Rajanna, "Novel approach to target cancer stem cells for therapy," *Medical Hypotheses*, vol. 88, pp. 83–85, 2016.

[46] Y. Wang, Y. Liu, J. Jiang, and H. B. Cui, "A new method for purification and identification of hepatocellular carcinoma stem cell of SMMC-7721," *Zhonghua Yi Xue Za Zhi*, vol. 92, no. 48, pp. 3434–3437, 2012.

[47] S.-C. Dang, X. Qian, W. Jin, L. Cui, J. Chen, and M. Gu, "G-protein-signaling modulator 2 expression and role in a $CD133^+$ pancreatic cancer stem cell subset," *OncoTargets and Therapy*, vol. 12, pp. 785–794, 2019.

[48] E. K. Park, J. C. Lee, J. W. Park et al., "Transcriptional repression of cancer stem cell marker CD133 by tumor suppressor p53," *Cell Death & Disease*, vol. 6, no. 11, article e1964, 2015.

[49] A. M. Mercurio, "VEGF/neuropilin signaling in cancer stem cells," *International Journal of Molecular Sciences*, vol. 20, no. 3, p. 490, 2019.

[50] C. Chen, S. Zhao, A. Karnad, and J. W. Freeman, "The biology and role of CD44 in cancer progression: therapeutic implications," *Journal of Hematology & Oncology*, vol. 11, no. 1, p. 64, 2018.

[51] Z. F. Yang, D. W. Ho, M. N. Ng et al., "Significance of CD90+ cancer stem cells in human liver cancer," *Cancer Cell*, vol. 13, no. 2, pp. 153–166, 2008.